

Origin of martian northern hemisphere mid-latitude lobate debris aprons

Han Li *, Mark S. Robinson, Donna M. Jurdy

Department of Geological Sciences, Northwestern University, Evanston, IL 60208, USA

Received 31 August 2004; revised 1 February 2005

Available online 15 April 2005

Abstract

Lobate debris aprons in the martian mid- to high-latitudes (northern and southern hemispheres) have been interpreted as ice-related features that indicate periglacial climate conditions as recently as late Amazonian. Using MOLA topographic profiles perpendicular to apron flow fronts, we surveyed 36 debris aprons in the northern hemisphere found in the regions of Mareotis, Protonilus, and Deuteronilus Mensae and Acheron Fossae. The profiles of these aprons were compared with idealized simple plastic and viscous power law models for ice-rock mixtures. All aprons studied exhibit convex profiles similar to a simple plastic model. This confirms previous interpretations that debris aprons are ice-rich mixtures with rheologies similar to stagnant ice sheets, thus indicating high ice concentrations (>40% by volume). About 60% of the surveyed debris apron population significantly deviates from the idealized simple plastic model profile; this may be due to locally reduced ice content, which primarily controls apron topography. Although post-emplacment modification due to near-surface ice sublimation plays a secondary role in defining the overall shape of aprons, it causes conspicuous surface textures. Degradation by ice sublimation probably results in pitted and ridge-and-furrow surface textures revealed by high resolution MOC images. Such textures may indicate decreased near-surface ice stability since the formation of the aprons, possibly due to Mars' current low obliquity after their emplacement. High ice content inferred from topography suggests some debris aprons have ice cores: potentially exploitable water resources for future robotic/human operations that could prove invaluable for missions remote from polar regions.

© 2005 Elsevier Inc. All rights reserved.

Keywords: Mars; Surface; Climate; Geological processes; Geomorphology

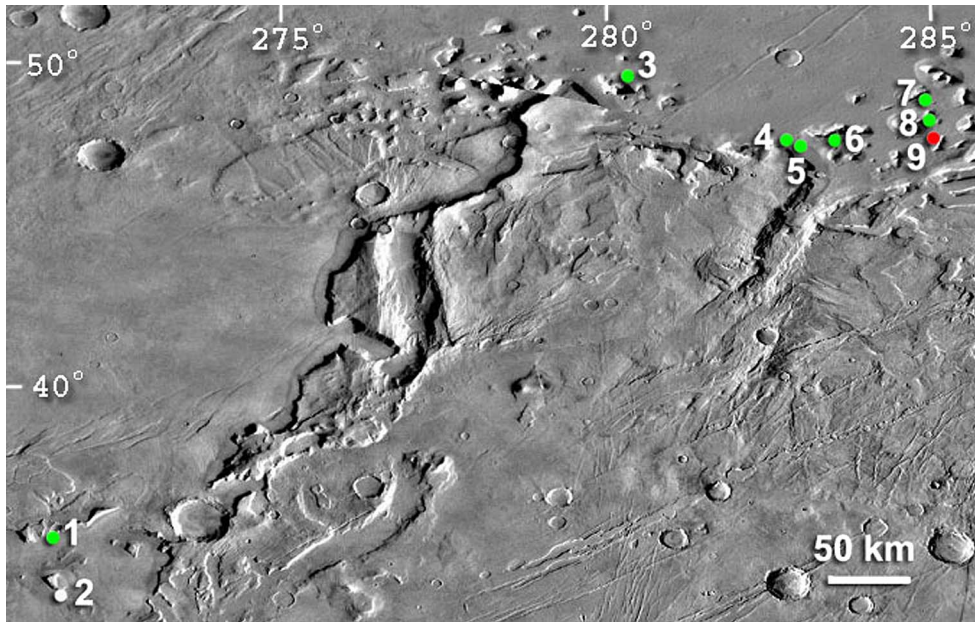
1. Introduction

Martian debris aprons are thick, gently sloped deposits of material that occur in mid- to high-latitude ranges in both the northern and southern hemispheres. Found at the bases of escarpments, they have distinctive lobate and convex profiles (Squyres, 1978). These features are generally interpreted to have formed due to ice-lubricated creep, and they have undergone a history of surface degradation through subsequent loss of ice (e.g., Squyres, 1978; Lucchitta, 1984; Crown et al., 1992). Current knowledge of debris aprons comes mainly from studies of their morphology and distribution pattern, however a quantitative understanding of their rheological nature remains unclear. To investigate their rheological characteristics, Mangold and Allemand (2001) com-

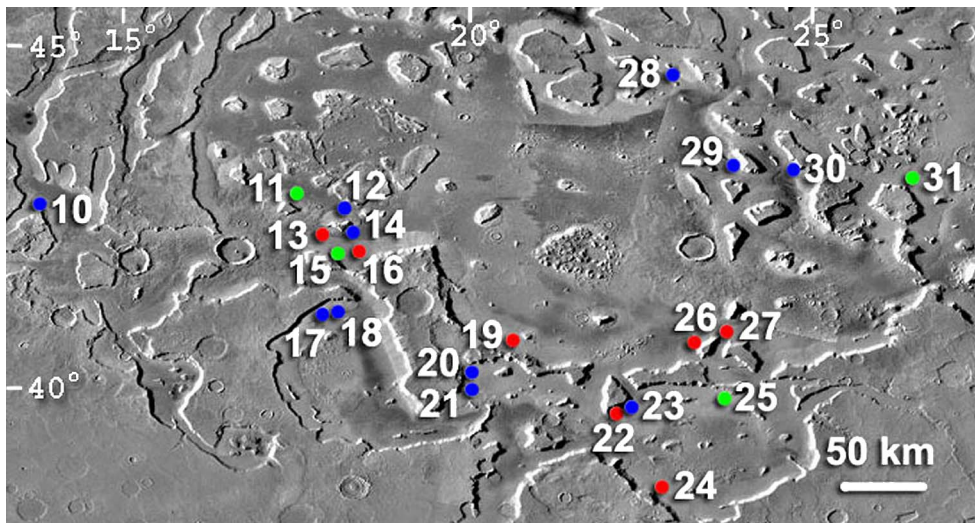
pared MOLA topographic profiles of five debris aprons from Deuteronilus and Protonilus Mensae with simple plastic and viscous power law models. Through topographic and volumetric analysis, these authors concluded that debris aprons originated from massive landslides and are due to the solid-state deformation of ice. Due to incomplete MOLA data available at that time, the analysis of Mangold and Allemand (2001) was limited to five debris aprons located within 40–46° N and 22–50° E. New MOLA data allow us to extend their analysis to the whole northern hemisphere. Employing the same rheological models as presented by Mangold and Allemand (2001), we compared longitudinal profiles of debris aprons from Mareotis, Protonilus, and Deuteronilus Mensae (Fig. 1), and Acheron Fossae with profiles of theoretical models and of water-based flows and dry landslides. Our expanded analysis tests the previous interpretation that debris aprons were formed due to deformation of ice-rock mixtures. We compared the profiles of 36 debris aprons with

* Corresponding author. Fax: +1 847 491 8060.

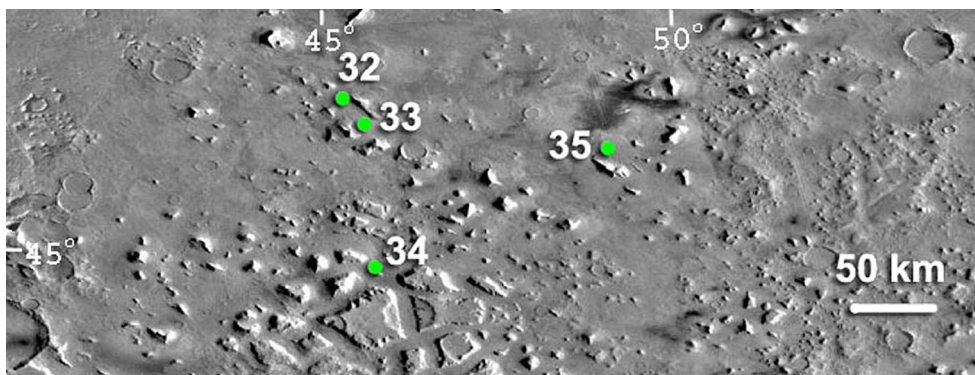
E-mail address: han@earth.northwestern.edu (H. Li).



(a)



(b)



(c)

Fig. 1. Debris aprons in (a) Mareotis Mensae (centered at 46° N, 278° E), (b) Deuteronilus Mensae (centered at 41.5° N, 20° E), and (c) Protonilus Mensae (centered at 45° N, 47.5° E). Labels indicate aprons analyzed in this study. Refer to Table 1 for the MOLA track number, location, and measurements of each debris apron. Base maps from USGS Mars Global Digital Image Mosaic (MDIM) version 2.1 with a resolution of 64 pix/degree. Map (a) is part of quadrangle MC-3 (Arcadia). Maps (b) and (c) are parts of quadrangle MC-5 (Isenius Lacus). North is up.

the predictions of simple plastic and viscous power law models. From our morphological study, we seek to establish whether high ice content in these deposits is required, and whether degradation processes have been active on these debris aprons after emplacement.

1.1. Lobate debris aprons

Martian lobate debris aprons, along with lineated valley fill and concentric crater fill, comprise a suite of features found in mid-latitudes of Mars that have been attributed to flow of ice-rich material (Fig. 2). They all exhibit young surface ages of Late Amazonian epoch (Squyres, 1978; Lucchitta, 1984). Ridge-and-furrow lineations radiate outward from the base of the escarpments on the surface of many of the debris aprons. Where the debris is confined, as in a valley, surface lineations are restricted to the flat valley floor and occur roughly parallel to the valley walls. Debris aprons are concentrated in two latitudinal bands 25° wide and centered on 40° N and 45° S, specifically the fretted terrain and fractured highlands of the northern hemisphere and areas surrounding the Argyre and Hellas Basins in the southern hemisphere (Squyres, 1979; Squyres and Carr, 1986; Pierce and Crown, 2003).

The size of debris aprons varies noticeably across the northern and southern hemispheres. In the northern hemisphere, the length of debris aprons can reach up to 33 km, and maximum thickness estimates vary between 620 and 900 m (Lucchitta, 1984; Squyres, 1989; Mangold and Allemand, 2001). In comparison, debris aprons in the southern hemisphere's eastern Hellas region extend laterally up to 50 km and attain maximum thickness up to 4 km, with an average thickness of ~1.2 km (Pierce and Crown, 2003).

The distinctive morphology and spatial distribution of debris aprons have inspired a variety of interpretations. In early works, Carr and Schaber (1977) postulated that debris aprons at the foot of isolated positive features in the Nilosyrtris, Protonilus, and eastern Hellas regions are formed by gelifluction or frost creep in a permafrost layer. They rejected an alluvial origin because the deposits are not fan shaped and do not exhibit evidence of gullying. A dry landslide origin also seemed unlikely because these debris aprons are not composed of discrete lobate flows. They attributed their formation to slow creep of debris away from a source area, facilitated by the freeze-thaw cycle of interstitial ice. Squyres (1978) questioned gelifluction as being responsible for debris aprons by pointing out that, first, the thick lobate morphology suggests that the movement involved a significant part of the deposit body rather than a thin surface layer; and second, no evidence exists for thawing to any significant depth. Instead, Squyres (1978, 1979) ascribed debris aprons to the deformation and flow of a mass consisting of erosional rock debris and ice incorporated from the atmosphere, analogous to terrestrial rock glaciers. Based on measurements from Viking orbital photographs and a plastic deformation model, Squyres (1978) estimated the yield

stress of debris aprons in Nilosyrtris and Protonilus Mensae to range from 0.6 to 1.3 bar, in agreement with the measurements of 1 to 2 bar for terrestrial rock glaciers (Wahrhaftig and Cox, 1959).

Later studies proposed that lobate debris aprons are flows of ice-rock mixtures; however, mechanisms for the derivation of interstitial ice and source rock particles remain unclear. Two mechanisms are proposed for the derivation of rock particles:

- (1) progressive rock falls accumulated at the foot of scarps (Squyres, 1978; Colaprete and Jakosky, 1998) or
- (2) mass wasting produced by landslides (Lucchitta, 1984; Mangold and Allemand, 2001).

From a morphologic point of view, Lucchitta (1984) proposed a landslide hypothesis to explain some particular scarp geometry with theater-shaped scarps. Mangold and Allemand (2001) estimated the volume of debris aprons and found this value is always greater than that expected of rock falls. Therefore the large volume of debris cannot be explained by rock falls alone, and only major landslides, involving ground ice or atmosphere-derived ice, can account for the large volume. Furthermore, Mangold and Allemand (2001) excluded the possibility of dynamic slumps like debris flows, because these flows would produce concave-shaped deposits, in contradiction with the observed topography. Thus the exact formation of these debris aprons still remains unclear.

Interstitial ice can have two origins: atmosphere or subsurface. Atmospheric frost can condense at the surface and percolate into debris (Squyres, 1978). In order for ice to survive the summer, it must be covered by debris coming from the surrounding plateau or air-borne dust and the atmospheric H₂O pressure must be higher than the subsurface H₂O pressure. However, Fanale et al. (1986) proposed that water frost only diffuses to several tens of centimeters in the ground, thus prohibiting the build up of significant ice laden source regions capable of producing aprons on the scale observed. Alternatively, Lucchitta (1984) suggested that ice is derived directly from the ground. Ground ice may be the relict of past aquifers charged by rainfall/nival activities and comes most probably from the subsurface of the plateau, over a thickness comparable to that of the scarp height, 1 to 2 km (Mangold and Allemand, 2001).

To constrain the mechanical characteristics of lobate debris apron material, several models have been proposed to simulate the flow state. Squyres (1978) proposed a plastic deformation model consistent with the known mechanical properties of terrestrial rock glaciers and with the observed morphology of the martian debris aprons. Employing a similar plastic model and adding the viscous power law model, Mangold and Allemand (2001) proposed that lobate debris aprons are due to solid-state plastic deformation of ice, after viscous flow deformation first occurred. Analyzing five MOLA topographic profiles, they found that the shapes of

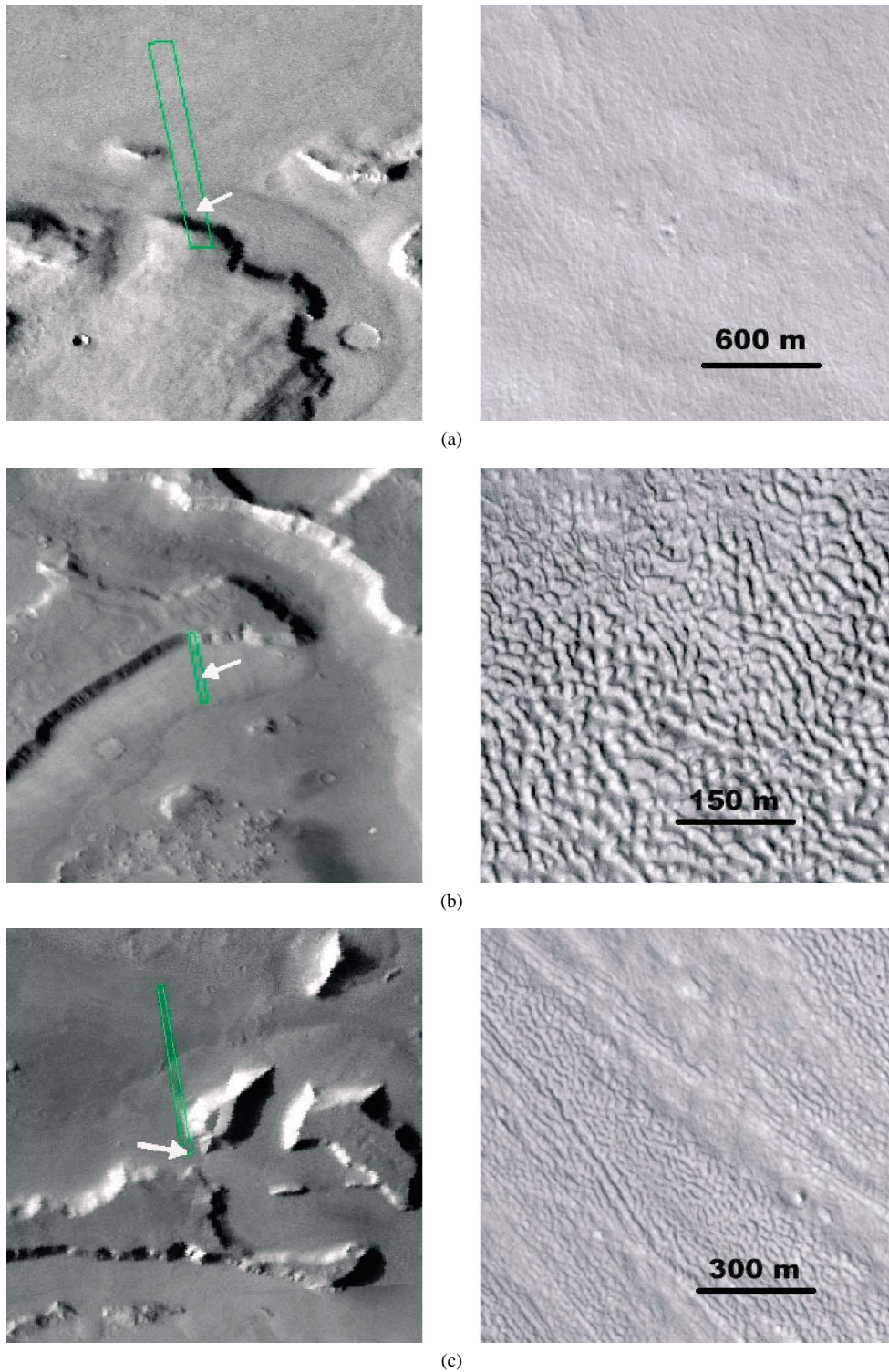


Fig. 2. Surface textures of debris aprons. Left column: MOC wide angle images as context (40 km wide), with white arrows indicating locations of narrow angle images. Right column: MOC narrow angle images showing surface textures. (a) Smooth surface texture (MOC image M0401207, 6 m/pix) may represent original apron surface; (b) pitted surface texture (MOC image FHA00877, 1.5 m/pix) may develop through ice sublimation induced collapse; (c) ridged texture (MOC image M704710, 3 m/pix). Sun is from the left. North is up.

debris aprons in Deuteronilus and Protonilus Mensae match the parabolic shape of theoretical profiles predicted for plastic ice sheets. Based on this observation, they excluded the possibility of basal sliding and sliding due to flows involved

with liquid, including mudflows and debris flows, because such processes would create concave profiles, which are inconsistent with the measured topography. However, this model itself cannot differentiate between a body made of

ice-rock mixture and a body made of ice; as long as they behave plastically (with ice content >40%), both bodies will have the same parabolic profile.

1.2. Ice-based terrestrial analogs

Rock glaciers or debris-covered glaciers on Earth exhibit numerous variety. For the purposes of this study we will adopt the rock glacier definition of Potter (1972): “a tongue-like or lobate body, usually of angular boulders, that resembles small glaciers, generally occurs in high mountainous terrain and usually has ridges, furrows, and sometime lobes on its surface, and has a steep front at the angle of repose,” acknowledging that rock glaciers have varied origins and flow processes.

Systematic study of terrestrial rock glaciers began with the work by Wahrhaftig and Cox (1959). Surveying 200 rock glaciers in the central Alaska Range, they estimated the apparent viscosity of these rock glaciers to be between 10^{11} and 10^{13} Pa s with maximum average shear stresses 1–2 bar. They proposed that rock glaciers constitute a continuum of landforms and require a near glacial climate to develop. To explain the flow mechanism, they suggested that rock glaciers move as a result of the flow of interstitial ice. Micro-relief features like longitudinal furrows and transverse ridges were studied in detail and were thought to result from the accumulation of ice-rich bands in the depressions between talus cones and shearing within the rock glaciers, respectively (Wahrhaftig and Cox, 1959).

Current models of rock glacier formation can be classified into three main categories, as discussed in detail by Whalley and Azizi (2003). Models include glacier-derived (Whalley and Martin, 1992), permafrost (e.g., Barsch, 1996; Haeblerli, 1985), and mass-wasting (landslide) (Johnson 1974, 1984; Whalley, 1983) origins. The glacial model assumes that ice comes from glacial sources preserved by an insulating rock debris layer. The thickness of the debris and local climate conditions dominantly control the preservation of the buried ice, therefore the distribution of rock glaciers depends on both: latitude and elevation. In the permafrost model, sub-surface ice either comes from ice segregation or seasonal frost. Requiring a periglacial temperature environment to form ground ice, this model implies that these features are generally confined to mid- to high-latitudinal bands. Finally, the landslide model suggests that rock glaciers are formed due to landslides or catastrophic rock avalanches with the ice component being indigenous to the mass wasted material. In this case, periglacial conditions are also necessary to allow ice to exist in the original sources of mass wasting.

These three models for terrestrial rock glaciers have all been employed by previous workers to describe martian debris aprons (e.g., Squyres, 1978, 1979, 1989; Lucchitta, 1984; Crown et al., 1992; Colaprete and Jakosky, 1998; Mangold, 2003; Pierce and Crown, 2003). Detailed assessment of each model can be found in Pierce and Crown (2003). Regardless of the origin of ice, rheological models

have been employed to study the internal structure and climate conditions for the formations of rock glaciers on Mars. Colaprete and Jakosky (1998) estimated that to form rock glaciers of the size found on Mars (>20 km in lateral extent), temperatures of 20 to 40 K higher than present average mid-latitude temperatures (210 K) are required with ice content of no less than 80%. However, other studies suggest that rock glaciers have ice content as low as 50% (Ewing and Schenk, 1998) or ~30% (Costard et al., 2002).

1.3. Water-based flows and dry landslides

Water-lubricated flows and dry landslides each have distinctive concave longitudinal profiles. A common type of water-based flow is the debris flow, “a process by means of which granular solids, sometimes mixed with relatively minor amounts of entrained water and air, move readily on low slopes” (Johnson, 1970). The granular solids in debris flows are relatively immobile by themselves and flow only on steep slopes, but the addition of water and air can tremendously increase their mobility (Johnson, 1965; Johnson and Hampton, 1969; Bulmer et al., 2002). Terrestrial debris flows have velocities ranging from 0.5 to about 20 m/s, and their viscosities are estimated to be about 100 to 800 Pa s, compared to 1×10^3 Pa s for pure water at 293 K (Costa, 1984; Iverson, 1997). The typical yield strengths in terrestrial debris flows range from 10^2 to 10^3 Pa (Allen, 1997).

Small gullies on the walls of impact craters and valley systems on Mars are attributed to fluid-mobilized mass movement processes (Malin and Edgett, 2000; Costard et al., 2002). These gullies have morphologies similar to terrestrial periglacial debris flow: both have head alcoves in the source region, channels with lateral levees, and blunt terminations (Malin and Edgett, 2000). Mangold et al. (2003) estimated the average viscosity and range of velocities of materials in gullies over large martian dunes to be 740 Pa s and 1 to 7 m/s, which correspond to terrestrial debris flows with 10 to 40% water ice content.

Morphologies of landslide deposits in Valles Marineris resemble those of terrestrial dry-rock avalanches, with concave longitudinal profiles, hummocky surface topography and steep marginal scarps characteristic of avalanche deposits (McEwen, 1989). Note that the concave profiles of martian landslides often result from the concave shapes of their runout paths, regardless of the rheology of deposits. In this case, rheological characteristics of landslides depend on runout distance, final deposit slope and thickness, and the shape of the deposit terminus (e.g., Harrison and Grimm, 2003). Assuming a Bingham model, McEwen (1989) estimated the yield strength of these landslides to be of 10^4 to 10^5 Pa, consistent with that of terrestrial dry rock avalanches. He also found that at a given value of H/L (height of drop/length of runout), the martian landslides are about 50 to 100 times more voluminous than terrestrial counterparts, consistent with the low gravity on Mars and the high yield strengths of these landslides. By comparing

model profiles with those of terrestrial, lunar, and martian landslides, [Harrison and Grimm \(2003\)](#) rejected the Bingham rheology for Valles Marineris landslides and argued for a general fluidization rheology, although they derived similar yield strength values for Valles Marineris landslides as those estimated by [McEwen \(1989\)](#). In the general fluidization model, the slides are frictional on failure but become fluidized when sufficiently energetic, thus behaving more like a power-law fluid. [Harrison and Grimm \(2003\)](#) proposed that the fluidization might be due to liquid water under a thin cryosphere or flash sublimation of CO₂ from the soil on failure, since the thin martian atmosphere is unlikely to provide sufficient lubrication. However, lunar landslides are well fit by an acoustic fluidization model ([Melosh, 1979](#)), despite the dessicated vacuum environment. In both wet and dry landslides, regardless of the shape of their runout paths, the final morphology of deposits is concave in profile and thus unambiguously different from those of martian debris aprons.

2. Rheological models and analysis

To characterize the rheological properties of debris aprons and investigate their formation and evolution, two models of ice sheets are used assuming the laws of simple plastic and viscous power behavior ([Mangold and Allemand, 2001](#)). In both cases, the basal shear strength σ_b can be expressed as ([Squyres, 1978; Paterson, 1994](#)):

$$\sigma_b = -\rho gh \, dh/dx, \quad (1)$$

where h and x are the thickness and radial length of the ice sheet, respectively, ρ is the density of ice or ice-rich regolith ($2.0 \times 10^3 \text{ km/m}^3$), and g is the gravitational acceleration (3.7 m/s^2 on Mars). The profile of an ice sheet is represented by ([Paterson, 1994](#))

$$(h/H)^2 + (x/L) = 1 \quad (2)$$

in the case of plastic equilibrium, or

$$(h/H)^{2+2/n} + (x/L)^{1+1/n} = 1 \quad (3)$$

in general, where H and L are the maximum thickness and maximum radial length of the ice sheet, respectively, and n is a constant that mainly depends on applied stress and ice purity. When $n \rightarrow \infty$, Eq. (3) reduces to Eq. (2). Previous workers ([Russell-Head and Budd, 1979; Lucchitta, 1984; Squyres, 1989; Paterson, 1994](#)) have suggested that n equals 3 for pure ice when stresses exceed 100 kPa. To reach this level of stress at the base of ice sheets on Mars requires an ice sheet at least 30 m thick. All flows under investigation in this study are thicker than 30 m, therefore, a value of n equals 3 is assumed. How ice purity affects ice creep is not fully understood ([Swinzow, 1962; Paterson, 1994](#)). Laboratory experiments show that when ice content exceeds 90%, the value of n is nearly equivalent to pure ice ([Hooke et al., 1972; Durham et al., 1992;](#)

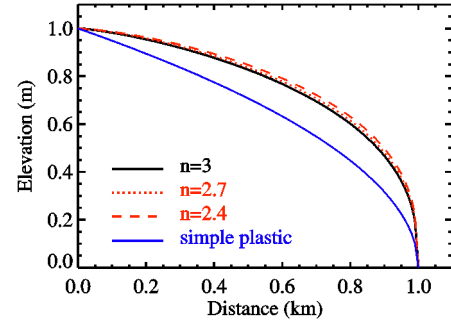


Fig. 3. Longitudinal profile predicted by viscous power law model when n varies within the range of 2.4 to 3. Variation shown of n due to varied debris concentration has small effect on the longitudinal profile of viscous materials. Therefore, assuming n to be a constant with the value of 3 is sufficient for the study of debris apron morphology. Black solid line represents $n = 3$, dashed line represents $n = 2.4$, and dotted line represents $n = 2.7$. As a comparison, simple plastic material is represented by blue solid line, always below viscous power law profile despite the variation of n within the viscous regime.

[Mangold et al., 1999](#)). However, at higher concentrations of solid inclusions (d), the creep rate of ice decreases ([Hooke et al., 1972](#)), and n should be modified to include this factor as follows: $n = 3 - d$ ($0 < d < 0.6$).

Based on Eqs. (2) and (3), we show the profiles predicted by simple plastic and viscous power law model in [Fig. 3](#), where $n = 2.4, 2.7$, and 3.0 for viscous model. In fact, within the viscous regime ($2.4 \leq n \leq 3$) the effect of variation of n on the shape of the profile is small; thus we assume n to be constant with a value of 3 as sufficient for our study. When d exceeds 60% ($n < 2.4$) and solid particles in the ice come into contact with each other, the strain rate of the ice decreases greatly and discontinuously ([Swinzow, 1962; Goughnour and Andersland, 1968; Hooke et al., 1972](#)). In such mixtures, solid particles impede the movement of dislocations within ice crystals, thereby suppressing ice creep ([Phukan, 1985](#)) and an ice creep model no longer describes the morphology of such flows.

We surveyed the northern hemisphere for debris aprons with MOLA profiles crossing at normal or close to normal directions to the apron front and found 36 aprons with measurable profiles out of 71 northern hemisphere aprons ([Fig. 1, Table 1](#)). These aprons encompass the geographic area of 36° N to 50° N in latitude and 14° E to 285° E in longitude, with elevations ranging from -3.5 to 0.8 km . The dimension of these aprons varies from 6 to 26 km in length and 200 to 780 m in thickness. We normalized each MOLA profile to unit length and unit thickness and plotted all the normalized profiles together in [Fig. 4](#). The profiles all exhibit convex shapes and are evenly distributed within a narrow range.

3. Results and discussion

We compare each apron profile with the simple plastic model in order to classify our observations. The deviation of

Table 1
Statistics of lobate debris aprons

Region	Apron #	MOLA #	Lat. (° N)	Lon. (° E)	Median elevation (m)	Vertical drop (m)	Length (km)	Surface texture	Geological unit	Km to dichotomy	Type
MM*	1	AP17516	42.56	271.40	769	358	12.4	–	Npl1	90	II
MM	2	AP18308	41.63	271.40	832	305	13.9	–	Nb–Nblh	56	–
MM	3	AP12479	49.75	280.18	–2580	450	10.0	–	Nplh	23	III
MM	4	AP12372	48.64	282.86	–2652	669	17.0	Smooth	Npl1–As	0	II
MM	5	AP15491	48.63	282.93	–2695	568	15.5	–	Npl1–As	0	II
MM	6	AP13900	48.78	283.49	–2772	361	9.4	Smooth	Nb	24	II
MM	7	AP18584-3	49.44	284.92	–3017	292	6.4	–	Nb	64	II
MM	8	AP18584-2	49.05	285.00	–2972	358	8.5	–	Nb	38	I
MM	9	AP18584-1	48.74	285.06	–3061	296	7.3	–	Nb	26	III
DM [†]	10	AP00260	42.54	13.81	–3365	521	17.1	–	Hr–As	0	I
DM	11	AP13073	42.78	17.53	–3465	380	10.2	Ridged	Hch	78	II
DM	12	AP17726-3	42.54	18.29	–3406	421	8.3	–	Hr	64	I
DM	13	AP18587	42.14	17.89	–3362	490	11.7	–	Hch	45	III
DM	14	AP17726-2	42.31	18.33	–3527	213	3.4	–	Hch	50	II
DM	15	AP17726-1	41.97	18.39	–3203	702	24.5	–	Hr–As	33	II
DM	16	AP19988	41.98	18.52	–3257	749	22.4	–	Hr–As	33	II
DM	17	AP15450	41.15	18.00	–3327	292	12.7	Pitted	Hr–As	0	I
DM	18	AP18254	41.14	18.08	–3362	274	8.4	Pitted	Hr–As	0	I
DM	19	AP12595	40.68	20.85	–3382	376	13.6	–	Hr–As	83	III
DM	20	AP20170-1	40.19	20.28	–3008	573	25.1	–	Hr–As	33	I
DM	21	AP20170-2	40.15	20.28	–3047	584	23.5	–	Hr–As	30	I
DM	22	AP00390	39.82	22.25	–3240	703	30.1	–	Hch–As	36	III
DM	23	AP00445	39.80	22.35	–3291	463	23.8	–	Hch–As	36	I
DM	24	AP10086-1	38.54	23.05	–3364	500	26.0	–	Hr–As	0	II
DM	25	AP19994-1	39.88	23.72	–3367	379	11.5	–	Hch–As	61	II
DM	26	AP10086-3	40.76	23.02	–3435	456	12.4	Ridge/furrow	Hch–As	55	III
DM	27	AP19994-2	40.84	23.88	–3404	415	11.5	–	Hch–As	48	III
DM	28	AP00205	44.55	23.02	–3507	279	10.6	–	Hr–As	257	I
DM	29	AP10086-2	43.22	23.85	–3248	223	8.8	–	Hr–As	171	I
DM	30	AP14236	43.11	24.78	–3451	236	6.7	–	Hr–As	164	I
DM	31	AP12601	43.02	26.53	–3263	586	17.5	Ridge/furrow	Hr–As	98	I
PM [§]	32	AP13072	46.97	45.31	–2934	330	10.3	–	Apk	346	II
PM	33	AP16826	46.70	45.85	–2802	266	8.8	–	Apk	341	I
PM	34	AP15449	44.58	45.95	–2143	685	15.4	Ridge/furrow, pitted, mounded	Npl2–As	236	II
PM	35	AP00245	46.45	49.06	–2646	778	22.4	–	Npl2–As	339	II
AF [#]	36	AP12135	35.84	229.52	78	194	10.0	–	Nf–Aa3	2400	I

Note: *MM = Mareotis Mensae; [†]DM = Deuteronilus Mensae; [§]PM = Protonilus Mensae; [#]AF = Acheron Fossae. Description of geology units: As = slide material; Aa3 = lowland terrain materials northern plains assemblage Arcadia Formation; Apk = knobby plains material; Hch = older channel, flood plain, and chaotic materials; Hr = ridged plains material; Npl1 = cratered unit; Nplh = hilly unit, resembles Nb but relief is gentler and faulting less intense; Nf = older fractured material; Nb = basement complex. Apron profile #2 represents an apron complex, therefore is not used for apron classification.

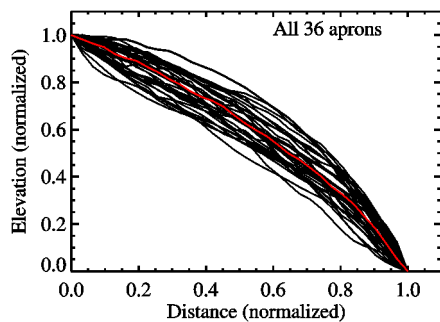


Fig. 4. Profiles of all 36 debris aprons in this study, normalized to unit length and thickness. Red represents median elevation.

the topographic profile with the model can be quantified by simply calculating the area between the real and model pro-

file. We calculate the differential area, A , between the normalized simple plastic model profile and a linear fit between the ends of this profile. We then classify each apron profile by comparing its differential area with the simple plastic model to A : type I $< A/3$, $A/3 \leq$ type II $\leq 2A/3$, type III $> 2A/3$ (Table 2). One apron profile fluctuates around the simple plastic model, and the image data show the MOLA profile passes over two overlapping aprons. Thus, the anomalous profile represents an apron complex rather than a single apron, so we eliminate this profile.

Composite profiles for each type of debris apron are compared with the simple plastic model (Fig. 5). To combine the profiles of a certain type, each profile is first normalized to unit length and height, then resampled to 31 data points. Thus, each data point can be represented as (x_i, y_i)

Table 2
Classification of lobate debris aprons

Type	Proportion	Total #
I	40%	14
II	40%	14
III	20%	7

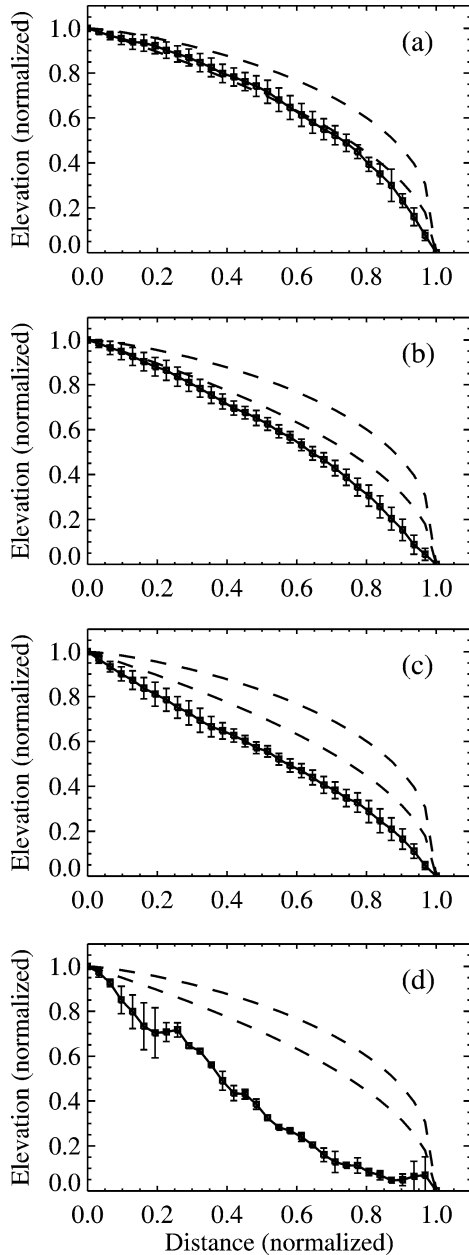


Fig. 5. Normalized composite profiles of: (a) type I lobate-shaped apron with convex profile that closely matches simple plastic model; (b) type II lobate-shaped apron with convex profile; (c) type III lobate-shaped apron with only slightly convex profile; and (d) landslides in Valles Marineris with profile of concave shape.

($i = 0, 1, 2, \dots, 30$), with x_i being the horizontal distance from the top of debris apron and y_i being the thickness, both in relative sense. Then, at each distance interval x_i , the me-

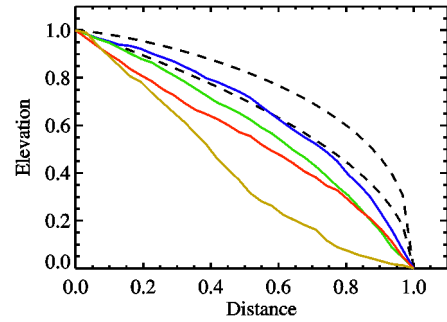


Fig. 6. Composite profiles of three types of lobate debris aprons and Valles Marineris landslides, normalized to unit length and thickness. Blue (highest solid curve) = type I ($n = 14$), green (second highest solid curve) = type II ($n = 14$), red (second lowest curve) = type III ($n = 7$), olive green (lowest curve) = Valles Marineris ($n = 3$). Lower and higher dashed lines represent simple plastic and power law model profiles, respectively.

dian and standard deviation of thickness y_i for all profiles belonging to the same type are calculated and are used to plot the composite profiles and their error bars, respectively. The thickness of each debris apron is taken to be equivalent to the vertical drop from its respective MOLA profile. By sampling ten aprons which appear to be emplaced on substrate with the highest slopes, we measured the regional slopes of the areas where debris aprons are distributed to be negligible ($< 1^\circ$). Thus, the substrate slope has very little effect on the final profile of a simple plastic material (Nye, 1952), therefore it is valid to assume the pre-existing basal slopes of debris aprons to be close to zero.

All types of debris aprons exhibit convex profiles and lie almost entirely below the simple plastic model. The composite type I profile best matches the simple plastic model, diverging in the lower reaches of the apron (Fig. 5a). Field studies of terrestrial rock glaciers suggest that increased steepness of the front is caused by positive ice mass balance or accelerated debris dumping to the front position (Whalley, 1983). However, such mechanisms are not likely to be applicable to martian conditions, since the fronts of lobate debris aprons are not as steep as the terrestrial rock glaciers and no morphological evidence exists for debris dumping at the front of debris aprons. The composite type II profile follows the overall parabolic shape of the simple plastic model, but plots below it (Fig. 5b). The composite type III profile deviates the most from the simple plastic model among these three, plotting even further below the model (Fig. 5c). In comparison, the composite profile of Valles Marineris landslides shows a distinctive concave shape and is well below both model and debris apron profiles (Fig. 5d).

The shape of longitudinal profiles of flow features is a manifestation of their rheology and provides important information regarding their composition and formation (Mangold and Allemand, 2001). The convex shape indicates that these debris aprons are composed of material with high yield strength, with ice-debris mixtures being the most likely candidate (e.g., Squyres, 1979; Lucchitta, 1984;

Mangold and Allemand, 2001) due to their morphological resemblance to terrestrial rock glaciers and their distribution in the mid- to high-latitudes. Yield strength values for these debris aprons estimated through quantitative analysis are in agreement with the above topographic analysis. By integrating Eq. (1) over the total length, L , and thickness, H , of the apron profile, the yield strength can be inferred from equation (Paterson, 1994)

$$\tau_b = \rho g H^2 / (2L). \quad (4)$$

Using the median length and thickness values for each type of aprons (10,300 and 325 m for type I, 13,900 and 380 m for type II, and 11,700 and 450 m for type III, respectively), and assuming density ρ to be $2.0 \times 10^3 \text{ kg/m}^3$, we estimate the yield strength of debris aprons to be 0.4–0.6 bar. This value is comparable to the yield strength measurements for terrestrial valley glaciers (0.5 bar) (Paterson, 1994), terrestrial rock glaciers (1 to 2 bar) (Wahrhaftig and Cox, 1959), and martian debris aprons in Nilosyrtis and Protonilus Mensae (0.6 to 1.3 bar) (Squyres, 1978). In addition, the convex profiles suggest that basal sliding is either lacking or is not a dominant process during the formation of debris aprons. If basal sliding occurred at the bottom of the ice sheets or ice-rock mixtures as they were forming, the movement would cause a concave shape of the deposits, as is often observed on terrestrial debris flows (Costa, 1984). Deviation from the parabolic profile of the simple plastic model suggests an important distinction in rheology between the debris aprons and the plastic model. As a whole, debris aprons seem to have higher viscosity than a simple plastic body. Since the relative high flow ability of debris aprons is due to ice cementing the rock debris, this deviation in rheology is most likely due to decreased ice concentration. Still, ice concentration should be higher than 40% in these debris aprons, otherwise rock particles would touch each other and behave rigidly (Swinzow, 1962), producing deposits similar to landslides or talus.

The majority of the aprons in the northern hemisphere are distributed at or near the southern highland–northern lowland dichotomy boundary, corresponding to the Contact 2 shoreline of Parker et al. (1993) and the late Noachian water table proposed by Head et al. (2004). Both the shoreline and the water table hypotheses provide possible sources for water ice in debris aprons. Type I aprons concentrate within Deuteronilus Mensae, a region at lower elevations compared to other locations in the northern hemisphere where debris aprons occur (Fig. 7a). If surface or ground water had existed in the past, it would have accumulated at lower elevations more easily and more ground water might have been preserved there. Therefore, Deuteronilus Mensae could have more water ice compared to other higher elevation locations, thus favoring type I apron formation. We use data from the Odyssey Neutron Spectrometer (NS) to test this hypothesis. NS measures the water equivalent hydrogen abundance in the upper meter of the surface in regions in Fig. 1a (Mareotis

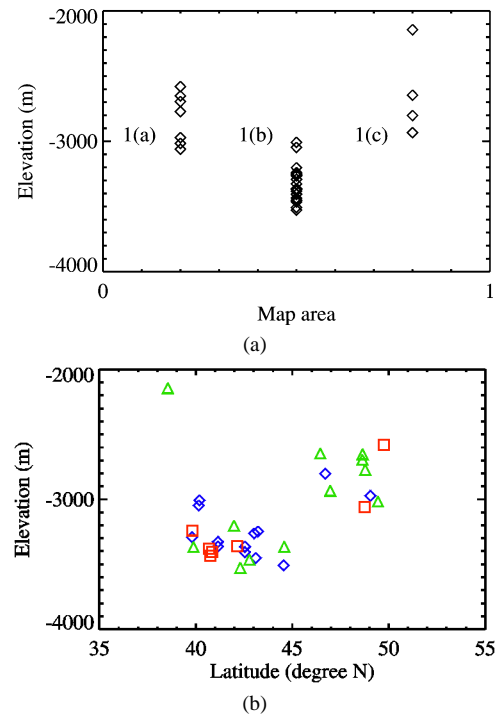


Fig. 7. Relationships between apron type and (a) elevation and (b) latitude (type I blue diamond shape, type II green triangle, type III red square).

Mensae), Fig. 1b (Deuteronilus Mensae), and Fig. 1c (Protonilus Mensae) to be comparable, each with 6, 6, and 4 wt% of water, respectively (Mitrofanov et al., 2002). Thus, NS data do not indicate significant variations in hydrogen between the three regions. The NS only measures the upper meter of the surface and current measurements do not necessarily indicate conditions at the time of the apron formation.

We suggest that local effects, like ice concentration and ice sublimation rate, possibly controlled by elevation, are important factors determining apron type. The deviation of types II and III apron profiles from the simple plastic model could be either primary (initial ice content variations upon emplacement) and/or secondary (post-emplacement ice volume changes) mechanisms. A primary mechanism for the glacier-origin model in types II and III aprons seems unlikely, since such features should exhibit profiles similar to debris-covered glaciers or ice-sheets which follow either simple plastic (type I) or viscous power law profiles. In periglacial or landslide models, a primary cause for types II or III is possible. The amount of ice formed in the pore space or ice contained originally in the landslide material is likely to vary locally. As experimental observations suggest, with a $\sim 5\%$ volume fraction of debris, the strain rate of dirty ice decreases to half of that of pure ice. With 40% volume fraction of debris, the strain rate of the ice-debris mixture is less by an order of magnitude than that of pure ice (Hooke et al., 1972). Lower ice content in source regions would result apron material with higher strength, causing apron deposits to resemble more closely landslide shapes (flatter profiles). Increased ice content ($>40\%$) in source regions increases

Table 3
Surface crater density of three types of debris aprons

Apron #	Apron type	MOC image #	MOC resolution (m/pix)	Crater density (#/km ²) of craters in certain diameter		
				<16 m	17–64 m	>64 m
18	I	FHA00877	1.5	11	0	0
1	II	M2301498	6	0	2.8	1.4
4	II	M0401207	6	38	3.2	0
6	II	M0204844	4.5	0	11.4	0
11	II	M1801821	5	4	0	0
23	I	M1002504	6	90	3	3
31	I	M1002711	3.7	4	0	2.1
34	II	M0903759	3.7	5.6	3.7	0
26	III	M0704710	3	1.3	0.9	0

the strain rate and reduces the strength of apron material, resulting in apron deposits with more convex profiles and resembling more closely glacial shapes.

Types II and III profiles may be the result of loss of internal ice after apron emplacement. Such a process is typical of terrestrial extinct debris-covered glaciers (Clark et al., 1994). Under current martian conditions, both ice core and interstitial ice can be lost to the atmosphere through sublimation. It is likely that after an extended period of time, enough ice, either originally in the state of ice lenses or interstitial ice, is released from the debris aprons to the atmosphere, causing a “deflated” appearance with profiles below the original parabolic shape. Assuming negative net mass balance for ice (more ice loss than gain), older aprons are expected to contain less internal ice and therefore exhibit less concave profiles compared with younger ones. Thus aprons with different shapes might represent different stages in their evolution. To test this hypothesis, we counted craters on 9 of our aprons that have high resolution MOC image coverage. Of the 9, only types I and III meet the criteria. Our crater counts (Table 3) did not suggest correlation between the surface age and type of debris aprons. However, due to limited high resolution MOC image coverage, this observation is not conclusive. McEwen (2003) cautions that such small area studies may be contaminated by secondary impacts and thus these relative counts are upper limits. More narrow-angle MOC images and future sub-meter resolution images by High Resolution Imaging Science Experiment (HiRISE) onboard Mars Reconnaissance Orbiter (MRO) are needed to better constrain the relative ages of debris aprons and to test whether differences in apron profiles represent consequent stages of apron evolution.

Atmospheric pressure and temperature are external factors that control the preservation of near surface ice. To test if the variations in these factors affect the evolution of aprons after emplacement, we compared elevations and latitudes of different aprons (Table 1, Fig. 7b). We did not find any definitive correlation between these factors and profile type. Although type II aprons seem to cluster around higher elevations and latitudes, there is not a continuous trend from types I, II, to type III, thus, we think the clustering of type II

is due to a random effect. Poleward orientation of debris aprons determines the solar influx reaching the apron surface. Under current martian conditions, northern hemisphere equator-facing slopes receive greater solar influx in the summer. During the orbital configuration Mars had high obliquity (Jakosky et al., 1995), the poleward-facing slopes in the northern hemisphere would be heated more in the summer. We found that 75% of type I aprons are equator facing, compared to 50% for type II aprons and 25% for type III aprons. Confidence interval tests establish the probability of type I being equator facing ranges from 52% to 98%, based on the available 14 data points of type I aprons and with a 95% confidence level. Similarly, the probability of type II (with 14 data points) being equator-facing ranges from 13% to 87%, and for type III (with 7 data points) 2% to 48%. Thus, our sample size is too limited to definitely determine the significance of the orientations. Solar influx may play an important role in the development of debris aprons and future study of more debris aprons in the southern hemisphere may clarify any potential orientation relationship. No correlation between apron size and type is found (Table 1). Small and large aprons may all have been emplaced and developed through similar mechanisms.

Surface morphology, such as pits and ridge-and-furrow texture, of upper apron material may indicate the loss of ice near the surface (Mangold et al., 2000; Mangold, 2003; Pierce and Crown, 2003). MOC narrow angle images show that surfaces of all three types of debris aprons often share similar smooth texture and sometimes exhibit ridged texture or pitted texture referred to as “basketball”-like by Malin and Edgett (2001) (Fig. 2). Smooth texture may be either of primary or secondary origin (Malin and Edgett, 2001). Meter-scale pits on mounded surfaces may have formed due to collapsing of the surface that is composed of dust and ice (Fig. 8). Such morphology is strikingly reminiscent of cockpit karst and cone karst developed in terrestrial limestone terrains. Cockpits are large, cone-shaped pits up to about 1 km in diameter that occur in tropical limestones which are formed largely by solution of the limestones and subsequent collapse along fissures (Sweeting, 1958). Residual rocks left at the intersection of several cockpits form steep-sided, cone-shaped hills that are separated by cockpits, giving rise to cone karst, or tower karst (Lehmann, 1936; Sweeting, 1958). Pitted texture is always adjacent to and lower than the smooth original surface. Thus, we theorize that pitted texture is formed by collapsing of the primary smooth dust-ice or rock-ice surfaces, following the formation of cavities below such surfaces as near surface ice is lost. Although terrestrial cockpit and cone karst formation and the pitted surface on debris aprons are formed by very different processes, with the former initiated by the intense solution of limestone and the later proposed to be due to loss of subsurface ice, both processes could lead to the collapse of unsupported ground, thus resulting in similar pit-and-hill morphology.

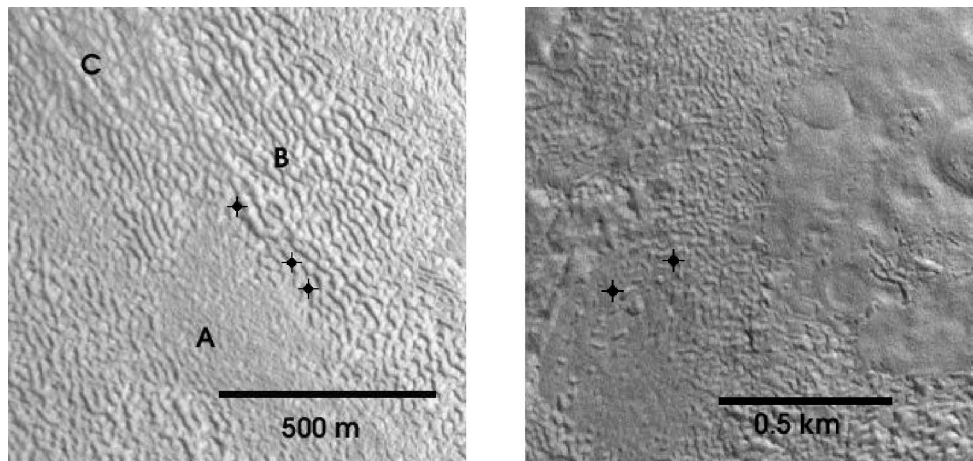


Fig. 8. Meter-scale pits (indicated by dots) on pitted texture surface develop from an originally smooth surface. Left: MOC image M0704710. Area B is interpreted to have developed from smooth area A due to pitting and further erosion led to the exposure of area C. Right: MOC image M0903759. Sun is from Southwest. North is up.

4. Summary and conclusions

Comparison between thirty six MOLA topographic profiles of martian northern hemisphere mid-latitude ($35\text{--}50^\circ$) debris aprons with rheological models for ice-rock mixtures reveals new insights into the formation of these features. This work expands the initial topographic study of five debris aprons presented by [Mangold and Allemand \(2001\)](#) to the whole northern hemisphere. Debris aprons exhibit convex profiles that closely match or follow the overall trend of the simple plastic model, suggesting these features are ice-rock mixtures with at least 40% (by volume) ice concentration. Such inferred high ice concentration is consistent with high water-equivalent hydrogen measurements made by the Odyssey neutron spectrometer ([Mitrofanov et al., 2002](#)). In fact ice concentrations $>20\%$ by volume occur in the top meter of some equatorial soils ([Boynnton et al., 2002](#)). Thus it is plausible that areas where debris aprons occur have similar concentrations of ice, but at depths below a meter. From the production function of [Hartmann and Berman \(2000\)](#), our crater counting results ([Table 3](#)) establish that northern hemisphere debris aprons have a young surface age less than 100 Myr. The key point here is that these features are geologically young. We note that current climate conditions in martian mid-latitudes are not optimal for recharging source regions and thus we infer that climate in the mid-latitudes of Mars was wetter than today—when the majority of aprons formed (<100 Myr). Distinctive pitted, and ridge-and-furrow surface textures may indicate surface collapse due to ice sublimation. They thus provide evidence for decreased stability of near-surface ice since their formation, and may point to a current interglacial period as proposed by [Head et al. \(2003\)](#).

Are debris aprons currently forming? We have found no evidence confirming the formation of new debris aprons. From the above observations, we can not exclude the scenario that debris aprons are currently forming. Based on the above lines of evidence, we prefer the hypothesis that

morphologies represented by the different types of aprons are primary. Secondary, i.e. post-emplacment, processes such as ice sublimation are more likely to result in surficial modification ([Mangold, 2003](#)) and do not control the overall profile shape of debris aprons. It is possible that once enough near surface ice has sublimated and the overlying debris reached a certain thickness limit, ice sublimation rate ceases and prevents further modification. Radar sounding data from Mars Advanced Radar for Subsurface and Ionosphere Sounding (MARSIS) onboard Mars Express may provide subsurface ice concentration 2–3 km into martian crust with horizontal resolutions of 5–10 km and vertical resolutions of 50–100 m in subsurface ([Picardi et al., 2004](#)). Shallow Subsurface Radar (SHARAD) onboard MRO will penetrate up to 1 km into martian crust to look for ice, with a resolution of 0.3–3 km horizontally and 15 m vertically ([Seu et al., 2004](#)). Such data sets will be of high enough resolution to detect if types II and III debris aprons (500–1000 m thick) have lower ice concentrations compared to type I aprons, and thereby test the hypothesis that the overall morphology of debris aprons is affected by secondary degradation processes.

Abundant ground ice possibly preserved in mid-latitude debris aprons represents potentially exploitable water reservoirs to sustain future robotic or human operations on Mars. Type I aprons, which we hypothesize to have the highest ice content, may contain the richest ice cores under debris cover, and are therefore high priority targets for water ice exploration.

In summary, through this study we have found that:

- 36 lobate debris aprons in martian northern hemisphere exhibit convex profiles that closely match or follow the profile of the simple plastic model.
- Ice-rock mixture is the most likely material that composes apron deposits, which are inferred to have a high ice content of $>40\%$ by volume.

- The types of apron profile may be correlated to varied ice concentration in aprons, with type I aprons possessing the highest ice content and type III the lowest.
- The differences in profile morphology and inferred ice concentrations are likely due to primary causes.
- Crater counting based on limited image data suggests that debris aprons are young features with an age constrained to be <100 Myr. Current climate conditions on Mars are not conducive for the formation of debris aprons. Thus, the climate at mid- to high-latitudes of Mars (100 Myr ago) must have been wetter and was probably similar to that of terrestrial periglacial regions.

Acknowledgments

The authors thank the editor and Keith Harrison and Francois Costard for their thorough reviews. This research was supported by NASA Grants NAG5-8294 and NAG5-12157 and Boos Graduate Fellowship from Northwestern University. MOLA data courtesy of NASA/GSFC. MOC images courtesy of NASA/JPL/Malin Space Science Systems.

References

- Allen, P.A., 1997. *Earth Surface Processes*. Blackwell, London.
- Barsch, D., 1996. *Rock Glaciers*. Springer-Verlag, New York.
- Boynton, W.V., 11 colleagues, 2002. Early results of the Mars Odyssey gamma-ray spectrometer (GRS), ice and other cool stuff. *Meteorit. Planet. Sci.* 37, Suppl. 21.
- Bulmer, M.H., Barnouin-Jha, O.S., Peitersen, M.N., Bourke, M., 2002. An empirical approach to studying debris flows: Implications for planetary modeling studies. *J. Geophys. Res.* 107 (E5), [10.1029/2001JE001531](https://doi.org/10.1029/2001JE001531).
- Carr, M.H., Schaber, G.G., 1977. Martian permafrost features. *J. Geophys. Res.* 82, 4039–4054.
- Clark, D.H., Clark, M.M., Gillespie, A.R., 1994. Debris-covered glaciers in the Sierra Nevada, California, and their implications for snow line reconstructions. *Squat. Res.* 41, 139–153.
- Colaprete, A., Jakosky, B.M., 1998. Ice flow and rock glaciers on Mars. *J. Geophys. Res.* 103 (E3), 5897–5909.
- Costa, J.E., 1984. Physical geomorphology of debris flows. In: Costa, J.E., Fleisher, P.J. (Eds.), *Developments and Applications of Geomorphology*. Springer-Verlag, Berlin, pp. 268–317.
- Costard, F., Forget, F., Mangold, N., Peulvast, J.P., 2002. Formation of recent martian debris flows by melting of near-surface ground ice at high obliquity. *Science* 295, 110–113.
- Crown, D.A., Price, K.H., Greeley, R., 1992. Geologic evolution of the east rim of the Hellas basin, Mars. *Icarus* 100, 1–25.
- Durham, W.B., Kirby, S.H., Stern, L.A., 1992. Effects of dispersed particulates on the rheology of water ice at planetary conditions. *J. Geophys. Res.* 97, 20,883–20,897.
- Ewing, R.C., Schenk, P.M., 1998. Formation of debris aprons on Mars; Viking stereotopographic mapping. *Lunar. Planet. Sci.* XXIX, Abstract 1543.
- Fanale, F.P., Salvail, J.R., Zent, A.P., Postawko, S.E., 1986. Global distribution and migration of subsurface ice on Mars. *Icarus* 67, 1–18.
- Goughnour, R.R., Andersland, O.B., 1968. Mechanical properties of a sand–ice system. *ASCE Soil Mech. Foundat. Division J.* 94 (SM4), 923–950.
- Haerberli, W., 1985. Creep of mountain permafrost: Internal structure and flow of alpine rock glaciers. *Mitt. ETH Zürich* 77, 1–142.
- Harrison, K.P., Grimm, R.E., 2003. Rheological constraints on martian landslides. *Icarus* 163, 347–362.
- Head, J.W., Mustard, J.F., Kreslavsky, M.A., Milliken, R.E., Marchant, D.R., 2003. Recent ice ages on Mars. *Nature* 426, 797–802.
- Head, J.W., Carr, M.H., Russell, P.S., Fassett, C.I., 2004. Martian hydrology: The late Noachian hydrologic cycle. *Lunar. Planet. Sci.* XXXV, Abstract 1379.
- Hartmann, W.K., Berman, D.C., 2000. Elysium Planitia lava flows; crater count chronology and geological implications. *J. Geophys. Res.* 105 (6), 15,011–15,025.
- Hooke, R.LeB., Dahlin, B.B., Kauper, M.T., 1972. Creep of ice containing dispersed fine sand. *J. Glacial.* 11, 327–336.
- Iverson, R.M., 1997. The physics of debris flows. *Rev. Geophys.* 35, 245–296.
- Jakosky, B.M., Henderson, B.G., Mellon, M.T., 1995. Chaotic obliquity and the nature of the martian climate. *J. Geophys. Res.* 100 (E1), 1579–1584, [10.1029/94JE02801](https://doi.org/10.1029/94JE02801).
- Johnson, A.M., 1965. A model for debris flow. Thesis, The Pennsylvania State University, Univ. Park, Pennsylvania.
- Johnson, A.M., Hampton, M.A., 1969. Sub Aerial and Sub Aqueous Flow of Slurries, Final Report to the US Gel. Survey. Banner Library, Stanford University, Stanford, CA.
- Johnson, A.M., 1970. *Physical Processes in Geology*. Freeman, New York.
- Johnson, P.G., 1974. Mass movement of ablation complexes and their relationship to rock glaciers. *Geogr. Ann.* 56A, 93–101.
- Johnson, P.G., 1984. Paraglacial conditions of instability and mass movement: A discussion. *Z. Geomorphol.* 28, 235–250.
- Lehmann, H., 1936. *Morphologische Studien auf Java*. Engelhorn. Geogr. Abhandl. 3 (9), 1–114. Stuttgart.
- Lucchitta, B.K., 1984. Ice and debris in the fretted terrain, Mars. *J. Geophys. Res.* 89, 409–418.
- Malin, M.C., Edgett, K.S., 2000. Evidence for recent groundwater seepage and surface runoff on Mars. *Science* 288, 2330–2335.
- Malin, M.C., Edgett, K.S., 2001. Mars Global Surveyor Mars Orbiter Camera: Interplanetary cruise through primary mission. *J. Geophys. Res.* 106 (E10), 23,429–23,570.
- Mangold, N., 2003. Geomorphic analysis of lobate debris aprons on Mars at MOC scale: Evidence for ice sublimation initiated by fractures. *J. Geophys. Res.* 108 (E4), [10.1029/2002001885](https://doi.org/10.1029/2002001885).
- Mangold, N., Allemand, P., Duval, P., Geraud, Y., Thomas, P., 1999. Ice content of martian permafrost deduced from rheology of ice-rock mixtures. *Lunar. Planet. Sci.* XXX, Abstract 1016.
- Mangold, N., Allemand, P., 2001. Topographic analysis of features related to ice on Mars. *Geophys. Res. Lett.* 28, 3407–3410.
- Mangold, N., Costard, F., Peulvast, J.-P., 2000. Thermokarstic degradation of lobate debris aprons and fretted channels. Second International Mars Polar Conference, Reykjavik, Iceland. Abstract 4030.
- Mangold, N., Costard, F., Forget, F., 2003. Debris flows over sand dunes on Mars: Evidence for liquid water. *J. Geophys. Res.* 108 (E4), [10.1029/2002001885](https://doi.org/10.1029/2002001885).
- McEwen, A.S., 1989. Mobility of large rock avalanches: Evidence from Valles Marineris, Mars. *Geology* 17, 1111–1114.
- McEwen, A.S., 2003. Secondary cratering on Mars: Implications for age dating and surface properties. Sixth International Conference on Mars, Pasadena, CA. Abstract 3268.
- Melosh, H.J., 1979. Acoustic fluidization: A new geologic process. *J. Geophys. Res.* 84, 7513–7520.
- Mitrofanov, I., 11 colleagues, 2002. Maps of subsurface hydrogen from the high energy neutron detector, Mars Odyssey. *Science* 297 (5578), 78–81.
- Nye, J.F., 1952. A comparison between the theoretical and the measured long profile of the Unteraar Glacier. *J. Glaciol.* 2, 103–107.
- Parker, T.J., Gorsline, D.S., Saunders, R.S., Pieri, D., Schneeberger, D.M., 1993. Coastal geomorphology of the martian northern plains. *J. Geophys. Res.* 98, 11,061–11,078.

- Paterson, W.S.B., 1994. *The Physics of Glaciers*, third ed. Elsevier, Oxford, UK.
- Phukan, A., 1985. *Frozen Ground Engineering*. Prentice Hall, New Jersey. 336 pp.
- Picardi, G., 12 colleagues, 2004. MARSIS: Mars Advanced Radar for Sub-surface and Ionosphere Sounding. MARS EXPRESS. The Scientific Payload. ESA publication SP-1240.
- Pierce, T.L., Crown, D.A., 2003. Morphologic and topographic analyses of debris aprons in the eastern Hellas region, Mars. *Icarus* 163, 46–65.
- Potter Jr., N., 1972. Ice-cored rock glacier, Galena Creek, northern Absaroka Mountains, Wyoming. *Geol. Soc. Am. Bull.* 83, 3025–3058.
- Russell-Head, D.S., Budd, W.F., 1979. Ice sheet flow properties from combined borehole shear and ice core studies. *J. Glaciol.* 24, 117–130.
- Seu, R., Biccari, D., Orosei, R., Lorenzoni, L.V., Phillips, R.J., Marinangeli, L., Picardi, G., Masdea, A., Zampolini, E., 2004. SHARAD: The MRO 2005 shallow radar. *Planet. Space Sci.* 52, 157–166.
- Squyres, S.W., 1978. Martian fretted terrain: Flow of erosional debris. *Icarus* 34, 600–613.
- Squyres, S.W., 1979. The distribution of lobate debris aprons and similar flows on Mars. *J. Geophys. Res.* 84 (B14), 8087–8096.
- Squyres, S.W., 1989. Urey prize lecture: Water on Mars. *Icarus* 79, 229–288.
- Squyres, S.W., Carr, M.H., 1986. Geomorphic evidence for the distribution of ground ice on Mars. *Science* 231, 249–252.
- Sweeting, M.M., 1958. The karstlands of Jamaica. *Geogr. J.* 24, 184–199.
- Swinow, G.K., 1962. Investigation of shear zones in the ice sheet margin, Thule area, Greenland. *J. Glaciol.* 4, 215–299.
- Wahrhaftig, C., Cox, A., 1959. Rock glaciers in the Alaska Range. *Bull. Geol. Soc. Am.* 70, 383–436.
- Whalley, W.B., 1983. Rock glaciers—Permafrost features or glacial relics? *Int. Conf. Permafrost. Proc.* 4, 1396–1401.
- Whalley, W.B., Azizi, F., 2003. Rock glaciers and protalus landforms: Analogous forms and ice sources on Earth and Mars. *J. Geophys. Res.* 108 (E4), [10.1029/2002JE001864](https://doi.org/10.1029/2002JE001864).
- Whalley, W.B., Martin, H.E., 1992. Rock glaciers, II, model and mechanisms. *Progr. Phys. Geogr.* 16, 127–186.